2014 IEEE International Conference on Robotics & Automation (ICRA)
Hong Kong Convention and Exhibition Center
May 31 - June 7, 2014. Hong Kong, China

Effect of Lug Sinkage Length to Drawbar Pull of a Wheel with an Actively Actuated Lug on Sandy Terrain

Yang Yang[1], Yi Sun[1] and Shugen Ma[1,2]

Abstract— **Sandy terrains are widely distributed on this planet and include desert, beach, and area affected by volcanic eruption where covered with ash. Currently, these environments still present a challenge for mobile robots due to their poor trafficability. One of the most essential requirements on such terrains for mobile robots is to generate enough drawbar pull with a small amount of slippage. For this purpose, protrusions or convex patterns called lugs (i.e. grousers) are attached on the wheels. However, oscillational drawbar pull generated by lugs results vibration of the robot body and therefore disturb the stability of the robot. In this paper, we aim to reduce the oscillation of the drawbar pull by proposing a novel wheeled mechanism integrated with an actively actuated lug. The drawbar pull on the sandy terrain in fabricated testbed is firstly measured on a prototype mechanism. Based on measured force, a strategy of tuning sinkage length of the active lug for generating stable drawbar pull is proposed. This method has the advantage of that it requires neither prior knowledge on terramechanic models nor physical properties of the terrain. The performance of the proposed method is finally verified by comparing the generated drawbar pull with that of a wheel with a fixed lug.**

I. INTRODUCTION

Wheeled robots have played a significant role in sandy environments for rescue or geological investigations. In such conditions, they easily slip or become mired in loose soil, even to the point of mission failure. Recently, especially with the developments of Mars/Moon exploration, significant efforts have been made for improving the traveling performance of wheeled robots on challenge terrains.

Attaching lugs to the wheel surface is an effective method for improving the traction performance of wheeled robots. For ease of turning, special tires with spiral fins were used on Micro5 [1]. The wheels of the Apollo lunar rover were studded with titanium chevrons to provide traction [2]. In addition to the pattern, the height of the lugs has an obvious influence on the driving performance of a wheel. Increasing the lug height can increase the amplitude of drawbar pull of the wheel, but simultaneously brings larger oscillation in it [3]. Sutoh et al. modelled the linear traveling speed of a wheel rover with grousers, and discussed the suitable lug interval on a wheel to weaken the oscillation for achieving stable linear velocity [4].

Many new mechanisms have been developed to overcome the limitations of conventional wheels studded with fixed lugs. Chen et al. introduced the concept of movable lugs for the driving wheel of a boat tractor [5]. Better pull and lift forces of the lugs could be obtained from this approach by setting the lug plates at an appropriate angle to produce the necessary forces. Experiments were conducted to observe and evaluate the lug forces acting on single movable lug [6]. The Intelligent Vehicle Group of Jilin University has developed a compound walking wheel having retractile laminas that can be extend and drawn back [7]. This wheel can passively adjust the protruded length of the laminas to provide traction for adopting environments. With the adjustment of the inclination angle or sinkage length of the lug, these new types of wheels displayed the effect of lug trajectory on soil-lug interaction forces. However, the lug trajectories achieved by these wheels are limited owing to the limitation of the degree of freedom of their mechanisms.

In addition to experimental investigation, many models have been proposed to model the wheel-soil interaction mechanics. Their principle was previously investigated by Bekker [8] and Wong [9]. Although, existing terramechanic models have been successfully applied to predict the wheel-soil interaction forces for smooth wheel, they can not inherently capture the fluctuations caused by lugs. To solve this problem, the discrete elements methods (DEM) have been applied to estimate the effect of the lugs [10]. Moreover, Irani et al. proposed a dynamic model to capture the dynamic oscillations observed for a wheel with lugs [11]. However, it is still intrinsically difficult to model the forces generating by the wheel having lugs, since their motion behavior of the wheel and lugs significantly affect each other.

In this paper, we measure the effect of lug sinkage length by using developed wheel with an actively actuated lug and further highlight the advantages of planning the lug sinkage length for improving the traction performance on a sandy terrain. The paper is organized as follows. A novel wheel towards accessing sandy terrain is presented in Section II. The measurement methodology is introduced in Section III. In Section IV, we measure the effect of lug sinkage length with the fabricated prototype and propose a strategy to adjust lug sinkage length for achieving stable drawbar pull. Finally, the conclusion and plans for future studies are presented in Section V.

II. WHEEL WITH AN ACTIVELY ACTUATED LUG

A. Mechanism and Prototype

To reduce the fluctuation of the drawbar pull of the wheel, we have developed a novel wheeled mechanism which has an actively controllable lug. The idea is inspired from our previous study on paddle trajectory generation method

[1]Y. Yang, [1]Y. Sun and [1]S. Ma are with the Department of Robotics, Ritsumeikan University, Shiga, 525-8577, Japan. Email: shugen@se.ritsumei.ac.jp (S. Ma)

[2]S. Ma is also with School of Electrical Engineering and Automation, Tianjin University, 300072, China.

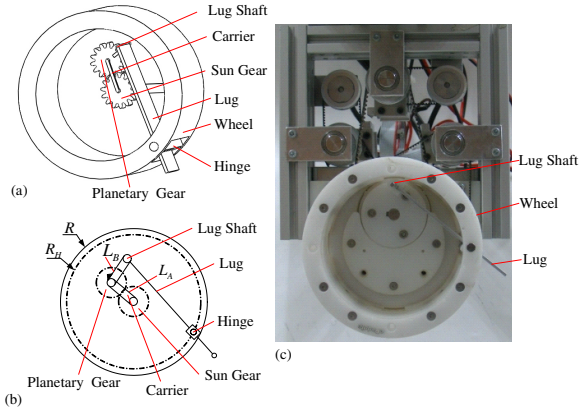

Fig. 1. Schematic of a wheel with an actively actuated lug: (a) mechanism, (b) kinematical diagram, (c) prototype .

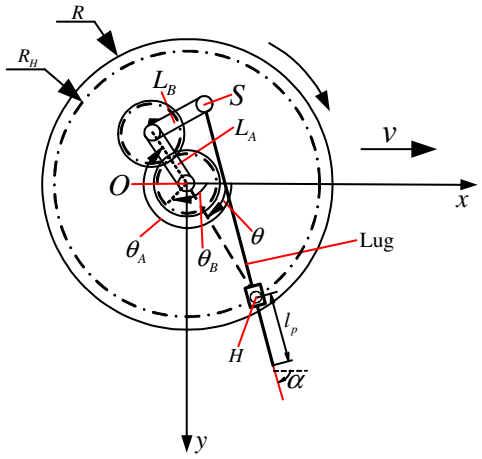

Fig. 2. Wheel coordinate system.

of ePaddle mechanism for accessing soft terrains [12]. As shown in Fig. 1, the mechanism consisting of a lug and a wheeled shell, has three degrees of freedoms. Its important components are presented as follow.

i) An active rotation joint for rotating the wheeled shell. The hinge can passively rotate around its shaft which is fixed on the wheel rim, to allow the lug to be retracted or protruded through the hinge freely.

ii) A planetary gear mechanism with a sun gear and a carrier that are respectively actuated by two motors to drive the lug shaft that is fixed on the planetary gear. The center distance between two gears, L_A, equals the center distance between the planetary gear and lug shaft L_B ; thus, the lug shaft can arrive at any position within the circle with a radius of $L_A + L_B$.

As the wheel is rolling forward, the lug can be actively protruded or retracted through hinge by changing the position of the lug shaft. The specifications of the wheel module are listed in Table I.

TABLE I
SPECIFICATION OF THE WHEEL MODULE.

Parameters	Value	Unit
Lug length L	93	mm
Lug width B	30	mm
Lug thickness	2	mm
Shell radius R	56	mm
Shell width	53	mm
Lug hinges layout circle radius R_H	50	mm
Center distance of planetary gear mechanism L_A	20	mm
Lug shaft layout circle radius L_B	20	mm

The wheel, carrier, and sun gear are driven by three DC brushed motors (RE25, Maxon Motor, Switzerland) via timing belts. Their angular positions are measured by three absolute encoders (RE22, RLS, Slovenia). Most of the components of the wheel module employed in this study were fabricated from polyoxymethylene (POM) using a laser cutter. This method significantly reduces the complexity, weight, and fabrication time and cost for prototyping. Fig. 1 (c) shows the fabricated prototype of the wheel.

B. Inclination Angle and Protruded Length

A wheel coordinate system on the sagittal plane of the wheel is defined as shown in Fig. 2; the origin is fixed at the wheel center, and the horizontal and vertical directions are denoted by x and y, respectively. The coordinate frame does not rotate with the driving motion of the wheel. On the basis of the three joint angles, the wheel joint angle θ, carrier rotation angle θ_A, and sun gear rotation angle θ_B, we can derive the protruded length l_p and inclination angle α of the lug. In the first step, the positions of the lug shaft S and the hinge H, are respectively described as

$$S = \begin{bmatrix} x_s \\ y_s \end{bmatrix} = \begin{bmatrix} L_A \cos\theta_A + L_B \cos(2\theta_A - \theta_B) \\ L_A \sin\theta_A + L_B \sin(2\theta_A - \theta_B) \end{bmatrix} \quad (1)$$

$$H = [x_H, y_H]^T = [R_H \cos\theta, R_H \sin\theta]^T \quad (2)$$

We then obtain the equations for calculating the length l_p protruded from the hinge in (3) and the inclination angle α of the lug in (4). The inclination angle is defined as the angle between the lug and the horizontal direction, as shown in Fig. 2.

$$l_p = L - \sqrt{(x_H - x_S)^2 + (y_H - y_S)^2} \quad (3)$$

$$\alpha = \text{atan2}(y_H - y_S, x_H - x_S) \quad (4)$$

There are three degrees of freedoms in the wheel module. As the wheel rotates at angle θ, we can control the position of the lug shaft to achieve desired inclination angle and the protruded length of the lug according to (5).

$$S = \begin{bmatrix} x_s \\ y_s \end{bmatrix} = \begin{bmatrix} R_H \cos\theta - (L - l_p)\cos\alpha \\ R_H \sin\theta - (L - l_p)\sin\alpha \end{bmatrix} \quad (5)$$

It should be noted that no solutions exist if S is out of the annulus with an inner radius of $L_A - L_B$ and an outer radius of $L_A + L_B$. Therefore, desired l_p and α are limited by (6), in which x_S and y_S are the functions of l_p and α described in (5).

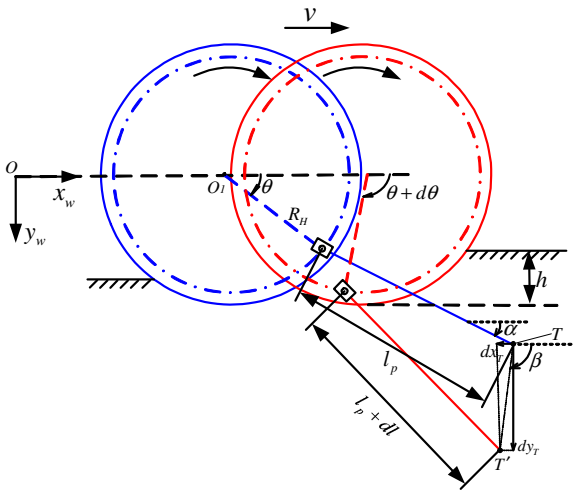

Fig. 3. Illustration of a single increment of lug displacement.

$$L_A - L_B \leqslant \sqrt{x_S^2 + y_S^2} \leqslant L_A + L_B \tag{6}$$

C. Tip's Moving Direction Angle and Lug Sinkage Length

Generally, slips occur when a vehicle travels on loose soil; it is expressed by the slip ratio s, that is defined as a function of the horizontal velocity of the wheel v, wheel radius R, and angular velocity of the wheel $\dot{\theta}$ as,

$$s = \frac{R\dot{\theta} - v}{R\dot{\theta}} \tag{7}$$

1) Tip's Moving Direction Angle: For a wheel rolling forward on soft terrain at constant slip ratio s and wheel sinkage h, the world coordinate system is established, as shown in Fig. 3. The horizontal and vertical directions are denoted by x_w and y_w, respectively. Given the angular position θ, the inclination angle α and the protruded length l_p, the position of the lug tip is described as follows:

$$\begin{aligned} x_T &= R\theta(1-s) + R_H\cos\theta + l_p\cos\alpha \\ y_T &= R_H\sin\theta + l_p\sin\alpha \end{aligned} \tag{8}$$

While the wheel rotates from θ to $\theta + d\theta$ and the protruded length changes from l_p to $l_p + dl$, the tip point moves from T to T' with infinitesimal displacements dx_T and dy_T, respectively. These can be derived by differentiating their position in (8), and then the tip's moving direction angle can be obtained as

$$\beta = \text{atan2}(dy_T, dx_T) \tag{9}$$

2) Lug Sinkage Length: The sinkage length determines the contact area between the lug and the soil. Before the lug completely sinks into the soil, its rear part is above the soil surface (Fig. 4 (a)), and thus, the sinkage length l_s is smaller than protruded length l_p. According to terramechanics, the soil-lug reaction force is generated as a result of the cohesion force and friction force at slip line TBCD (Fig. 4 (b)), which starts from the lug tip till an intersection point at the soil

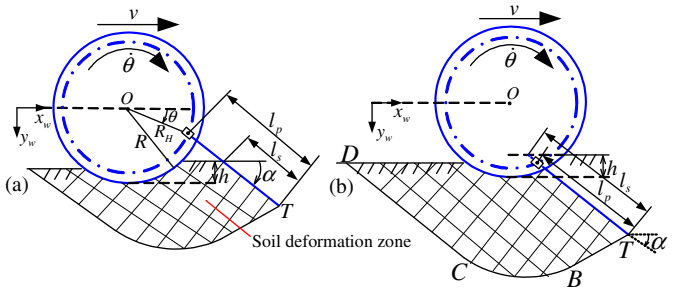

Fig. 4. Relationship between the protruded length l_p and sinkage length l_s when the lug has sunk into the soil (a) partly and (b) completely.

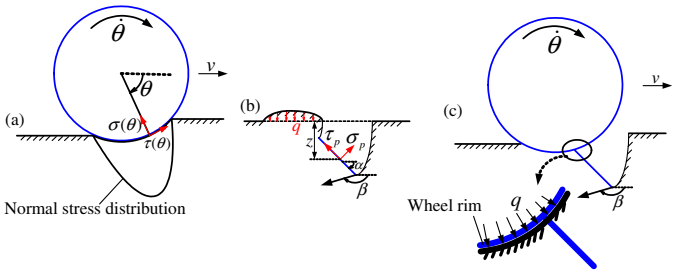

Fig. 5. (a) Wheel stress model, (b) lug stress model, (c) the interplay between the wheel and lug.

surface. The start point is determined by the depth achieved by the lug tip, so l_s is larger than l_p after the lug sinks into the soil completely. In both conditions, the sinkage length l_s can be calculated by using the y-coordinate of lug tip that represents the depth arrived at by the lug, as

$$l_s = \frac{y_T - (R-h)}{\sin\alpha} = l_p - \frac{R - h - R_H\sin\theta}{\sin\alpha} \tag{10}$$

D. Drawbar Pull

As the wheel rolls forward on a soft terrain, the drawbar pull is the sum of the forces acting on the wheel rim and the lug.

The common method for modelling the drawbar pull acting on the smooth wheel is by integrating the normal and shear stresses acting on the contacting surface of the wheel (Fig. 5 (a)). The normal stress and shear stress are calculated based on the Bekker's formula and Janosi - Hanamoto equation, respectively [9]. Its validity was verified by experiments in many reports.

The passive pressure theory is generally adopted to estimate the effect of the lug. According to equation (11), in addition to soil parameters (soil cohesion c, internal friction angle ϕ and soil density γ), the passive stress acting on a point belong to the lug, σ_p, is determined by its depth z and the surcharge q, as shown in Fig. 5 (b) [13].

$$\sigma_p = \frac{\gamma z N_\phi + q N_\phi + 2c\sqrt{N_\phi}}{\sin\alpha} \tag{11}$$

where N_ϕ is given by

$$N_\phi = \tan^2(45^\circ + \frac{\phi}{2})$$

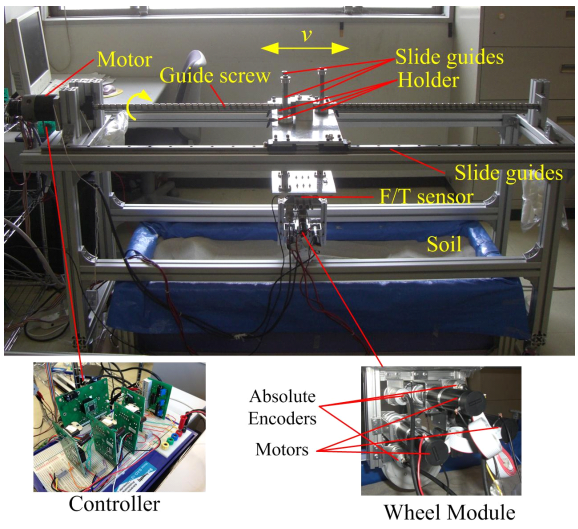

Fig. 6. Wheel-soil interaction testbed.

Then, the tangential stress can be calculated in (12).

$$\tau_p = c_a + \sigma_p \tan\delta \tag{12}$$

where c_a and δ are the soil-lug adhesion and friction angle, respectively.

It is however difficult to model their resultant effect of the wheel and the lug, since their motion behavior significantly affect each other. As shown in Fig. 5 (c), the wheel provides a normal stress q acting on the soil free surface that is as a surcharge to enhance the lug-soil interaction forces than single lug does. On the other hand, the normal and shear stresses acting on the wheel rim are changed by the motion of the lug that digs and changes the soil structure beneath the wheel. In this study, we conduct the experiments to measure the relationship of the drawbar pull and the lug sinkage length. Based on the measured results, we propose a strategy to achieve stable drawbar pull by adjusting the lug sinkage length during the wheel rotation without applying the terramechanic models.

III. DRAWBAR PULL MEASUREMENT TESTBED

The measurements were conducted in a testbed (Fig. 6) having a length of 1700 mm, a width of 500 mm and a height of 800 mm. The testbed comprises both a conveyance unit and a wheel-driving unit. The conveyance is actuated along two slide guides at desired speed by DC brushed servo motor via ball-bearing screw. An incremental encoder (E6A2-CWZ3E, OMRON, Japan) was used to feedback the angular position of the screw. The three motors (RE25 integrated with gearbox (GP26B), Maxon Motor, Switzerland) in the wheel module were controlled by a dsPIC33FJ128MC804-based controller (Microchip, USA) developed in our laboratory. The angular positions of the three joints was collected by three absolute encoders (RE22, RLS, Slovenia). The signals from one incremental encoder and three absolute encoders were sampled at a rate of 200 Hz via a digital input/output board (NI-6001, National Instrument, USA) on a PC running a Windows XP operating system. On basis of the data from the encoders, we can obtain the real trajectory of the lug. The wheel module and the conveyance unit were connected by a six-axis force/torque sensor (Mini 8/40, BL Autotec, Japan) that measures the drawbar pull of the wheel. The force signals were sampled by an A/D board (AD12-16(PCI), Contec, Japan) at the same sample rate as used in digital data acquisition for encoders.

The dry sand was used in the experiments, whose physical and mechanical properties are listed in Table II.

TABLE II
SOIL PARAMETERS.

Parameters	Value	Unit
Cohesion stress c	400	Pa
Soil friction angle ϕ	38.1	deg
Soil specific weight γ	1480	kg/m^3

IV. TUNING DRAWBAR PULL BY SINKAGE LENGTH OF THE LUG

A. Lug-soil Interaction Process

Wheel slips and sinks as rolling on soft terrain. To avoid such slippage and sinkage, we consider to control the sinkage length of the active lug at each angular position of the wheel to gain additional drawbar pull. A complete lug-soil interaction process is divided into three phases. In phase I, the lug penetrates the soil; and then it is driven to move along a desired trajectory in phase II. Lastly, the lug is retracted from the soil in phase III.

B. Effect of Lug Sinkage Length

Experiments were conducted to investigate the effect of the lug sinkage length on the drawbar pull. We measured the drawbar pull with lug sinkage lengths varied from 18 to 24 mm at an interval of 2 mm. In all experiments, the wheel sinkage was 5 mm; the wheel was rotating from 0 to 180 deg at constant angular velocity of 30 deg/s; the traveling velocity was 20 mm/s, thus the slip ratio was 0.3. In total, 10 trails were repeated in each configuration.

1) Lug Trajectory: In the first step, we summarize the procedure to determine the trajectory of the lug in phase II. As shown in Fig. 7, to isolate the effect of inclination angle, α is kept as 70 deg within this phase. Because the wheel sinkage and lug sinkage length are constant, the lug performs a translational motion with a moving direction angle of 180 deg and thus the trajectory of lug shaft forms a horizontal line inside its workspace. The initial rotation angle of the wheel in phase II is 22 deg in all experiments, and starting point S_1 can be derived according to kinematic model correspondingly. Destination S_2 of this phase is the interaction point of the trajectory of the lug shaft and its workspace boundary.

The lug shaft is initially positioned at S_1 before the wheel starts to rotate. In phase I, as the wheel rotates from 0 in constant angular velocity, the lug is forced by the hinge to penetrate the soil and then starts to push the soil backward. The α and l_s are continuously increasing to 70 deg and the

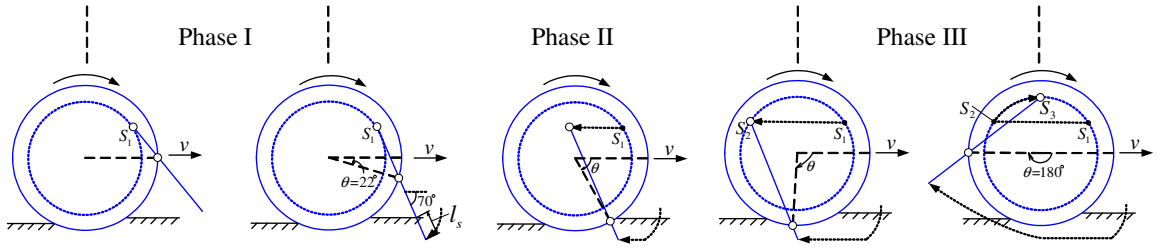

Fig. 7. Wheel-soil interaction process.

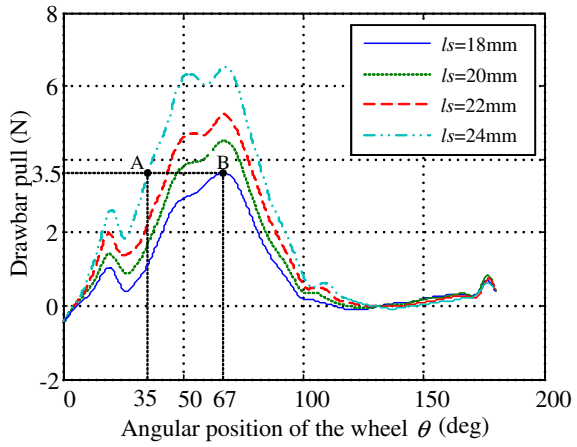

Fig. 8. Drawbar pull versus rotation angle of the wheel in different lug sinkage length.

desired sinkage length, respectively, as the angular position of the wheel increases to 22 deg. Subsequently, the lug shaft arrives at its initial position in phase II.

After the lug shaft arrived at S_2, it goes back to S_3 along the arc S_2S_3 at constant speed with the wheel rotation in phase III. When the wheel rotates to 180 deg, the lug shaft stops at S_3, exactly.

2) Experimental Results and Discussion: The mean values of drawbar pull over 10 trails for each configuration are plotted in Fig. 8. After the contact between the lug and the soil, the drawbar pull increased in phase I. There existed a slight decrease of the drawbar pull when the wheel is shifting from the Phase I to Phase II around 22 deg. The reason is that the velocity of the lug tip is discontinuous as the motion of the lug switches from phase I to phase II.

After a sharp increase during the first part of the Phase II, the drawbar pull slowly increased to its peak value at wheel rotational angle about 67 deg. Then, the force significantly dropped to a small value in rear period of phase II and phase III. It is deduced that as the lug is bulldozing the soil, the ground behind the lug trends to swell. However, the wheel inhibits this swell while applying a surcharge on the ground, thus it enhances the lug reaction forces as described in equation (11). As the lug moves backward further, more and more of the soil flow and swell behind the wheel and thus the effect of the wheel gradually disappears. As a result, the reaction force will decrease in this period.

Moreover, it can be seen that the wheel with larger sinkage length of the lug can generate larger drawbar pull. This phenomenon is easy to be explained based on existing terramechanic model as equation (11). Larger sinkage length can provide larger contacting area between the lug and soil.

C. Decrease of Oscillation in Drawbar Pull

1) Strategy: According to aforementioned experimental results, the force is not stable even though all the motion parameters (inclination angle, lug sinkage length and tip's moving direction angle of the lug) were kept constant. Based on the drawbar pull characteristics, a simple strategy to control the lug sinkage length to achieve stable drawbar pull is proposed in this study.

For example, if a desired drawbar pull of 3.5 N was given, we can draw a horizontal line on the Fig. 8, the leftmost interaction point, A (l_s=24 mm, θ=35 deg), and the rightmost interaction point, B (l_s=18 mm, θ=67 deg), were subsequently obtained. Therefore, the lug sinkage length in phase II was as follow: the lug was driven in constant sinkage length of 24 mm as the wheel rotates from 22 deg to 35 deg; and then the lug sinkage length linearly decreased from 24 mm to 18 mm as the wheel rotates from 35 deg to 67 deg; Lastly, it was kept as 18 mm until the end of phase II. The motion of the lug in phase I and III was as same as mentioned previously (Fig. 9 (a)).

2) Experimental Results and Discussion: As shown in Fig. 10, although the drawbar pull is approximately stabilized about 5 N in the range of [41 deg,72 deg] of wheel rotation angle, the value is however larger than desired value of 3.5 N. The curves in Fig. 8 and the results in Fig. 10 were derived by adopting constant and varied lug sinkage length, respectively. The different behavior caused the difference between the desired and actual values, since the wheel/lug interaction forces are significantly affected by accumulated deformation of soil that forms based on previous interaction procedure.

The other example is given in trajectory ii) as shown in Fig. 9 (b). It also can achieve stable drawbar pull within the range [41 deg, 70 deg] of wheel rotation angle. The stable value (about 4.2 N) is smaller than it generated in trajectory i). Therefore, it is possible to achieve force control by adjusting the lug sinkage length to make the wheel move with small amount of slippage. It is noteworthy that even though the stable range is small, using multiple controllable lugs and making them insert into the sand one by one could generate more wider range and more stable drawbar pull.

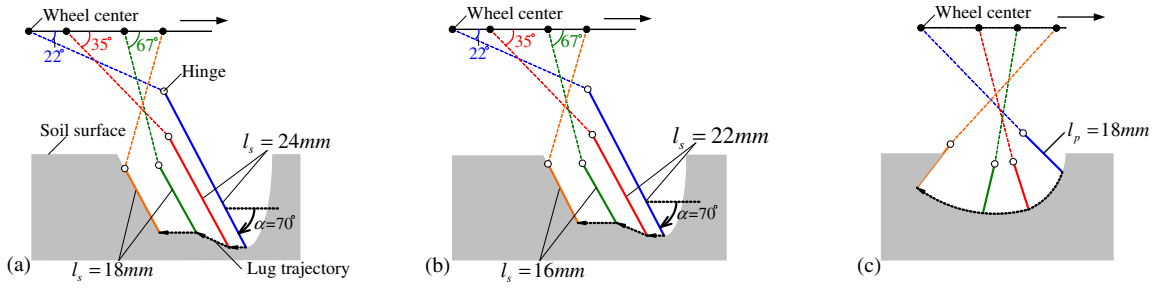

Fig. 9. Lug trajectory in experiments: (a) trajectory i), (b) trajectory ii), (c) fixed lug.

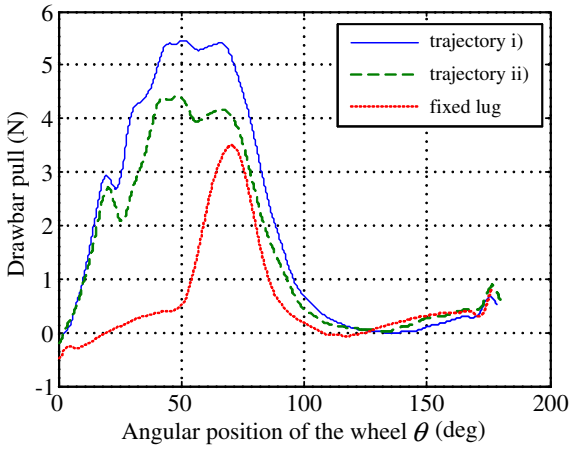

Fig. 10. Drawbar pull versus rotation angle in different lug trajectory.

To show the advantage of actively adjusting sinkage length of the lug further, the drawbar pull generated by using wheel with fixed lug of 18 mm height (Fig. 9 (c)) is plotted in Fig. 10. Before the lug contact the ground, slight drawbar pull was contributed by interaction of the smooth wheel and the ground. Then, after the lug reached the soil, drawbar pull rapidly increased to its peak value when the wheel rotated at 70 deg. After reaching that peak value, the drawbar pull rapidly decreased. The rapid increasing and decreasing of the drawbar pull on such a short period leads fluctuation in the traveling velocity of the wheel, and therefore reduce the stability of the robot. Comparing to the fixed lugged wheel, we find that the wheel with active lug is able to insert the lug into the soil earlier and depart from the soil later and generate a stable drawbar pull in a wider range.

In this study, we did not apply any terramechanic model. The strategy for controlling the lug sinkage length is based on the measurement of the drawbar pull generated by our developed wheel mechanism in Fig. 8. Therefore, the experimental study in this paper has potential to avoid the limitation in existing terramechanic model and to be applied in more kinds of soft terrains. It is also possible to adjust the drawbar pull on-line by controlling the lug sinkage length.

V. CONCLUSIONS

In this paper, we have developed a new form of wheel with a controllable lug and proposed a strategy to adjust the lug sinkage length to achieve stable drawbar pull. Its validity has been verified by experimentally comparing with conventional wheel with fixed lug. It is possible to achieve drawbar pull control by adjusting the lug sinkage length. Moreover, the proposed strategy did not based on any terramechanic model, thus it is expected to be applied in a wide range of soft terrains. In the coming studies, the effect of lug inclination angle will be studied to enhance the traction and flotation performance of our developed wheel module.

REFERENCES

[1] T. Kubota, Y. Kuroda, Y. Kunii, and I. Nakatani, "Small, light-weight rover "micro5" for lunar exploration," *Acta Astronautica*, vol. 52, no. 2-6, pp. 447 – 453, 2003.

[2] The apollo lunar roving vehicle. http://nssdc.gsfc.nasa.gov/planetary/lunar/apollo-lrv.html.

[3] L. Ding, H. Gao, Z. Deng, K. Nagatani, and K. Yoshida, "Experimental study and analysis on driving wheels' performance for planetary exploration rovers moving in deformable soil," *Journal of Terramechanics*, vol. 48, no. 1, pp. 27 – 45, 2011.

[4] M. Sutoh, K. Nagaoka, K. Nagatani, and K. Yoshida, "Design of wheels with grousers for planetary rovers traveling over loose soil," *Journal of Terramechanics*, no. 0, pp. 1 – 9, 2013.

[5] B. Chen and Y. Chao, "The research of driving wheel with movable lugs of the paddy field floating tractor," in *Proceedings of the 8th International Conference on International Society for Terrain-vehicle Systems (ISTVS1984)*, Cambridge, Aug. 1984, pp. 495 – 505.

[6] W. Hermawan, A. Oida, and M. Yamazaki, "Measurement of soil reaction forces on a single movable lug," *Journal of Terramechanics*, vol. 33, no. 2, pp. 91 – 101, 1996.

[7] Z. Chen, "Research of compound walking wheel having retractile laminas with application to lunar rover," Master's thesis, Jilin University, Changchun, China, (in Chinese) 2007.

[8] Bekker.M.G, *Introduction to terrrain-vehicle systems*, A. Arbor, Ed. The University of Michigan, 1969.

[9] J. Wong and A. Reece, "Prediction of rigid wheel performance based on the analysis of soil-wheel stresses part i. performance of driven rigid wheels," *Journal of Terramechanics*, vol. 4, no. 1, pp. 81 – 98, 1967.

[10] H. Nakashima, H. Fujii, A. Oida, M. Momozu, Y. Kawase, H. Kanamori, S. Aoki, and T. Yokoyama, "Parametric analysis of lugged wheel performance for a lunar microrover by means of dem," *Journal of Terramechanics*, vol. 44, no. 2, pp. 153 – 162, 2007.

[11] R. Irani, R. Bauer, and A. Warkentin, "A dynamic terramechanic model for small lightweight vehicles with rigid wheels and grousers operating in sandy soil," *Journal of Terramechanics*, vol. 48, no. 4, pp. 307 – 318, 2011.

[12] Y. Yang, Y. Sun, and S. Ma, "Paddle trajectory generation for accessing soft terrain by an epaddle locomotion mechanism," in *Proceedings of the 2013 IEEE International Conference on Robotics and Automation (ICRA 2013)*, Karlsruhe, Germany, May. 2013, pp. 403 – 408.

[13] J. Wong, *Theory of Ground Vehicles Third edition*. New York: Wiley-Interscience, 2001.